analytical chemistry

pubs.acs.org/ac Article

Universal Low-Background Fluorophore Platform via Structural Reprogramming of Oxazine 1 with Julolidine for Activatable Probe Design

Dianfeng Dai, Zhimin Zhang, Mo Ma, Chen Zhao, Jingkang Li, Siqi Zhang, Pinyi Ma,* Bo Zhang,* and Daqian Song*

Cite This: *Anal. Chem.* 2025, 97, 21071−21078 Read Online

ACCESS | Metrics & More | Article Recommendations | Supporting Information

ABSTRACT: Fluorescent probes play a vital role in biological detection and imaging; however, their application is often hampered by high background fluorescence, which compromises detection sensitivity and reduces the signal-to-noise ratio. Oxazine 1 is a modifiable near-infrared fluorophore that can be used to develop low-background probes. Nonetheless, it suffers from limitations such as insufficient red-shifted emission, low fluorescence quantum yield, and poor cellular uptake. To address these limitations, we designed and synthesized two new oxazine derivatives, JSO and JDO, by replacing the diethylamino donor group of oxazine 1 with a rigid julolidine moiety. This structural modification effectively enhanced electron-donating ability, suppressed nonradiative decay, and improved membrane permeability. Compared to oxazine 1, the emission wavelength of JDO was red-shifted (703 nm), and its fluorescence quantum yield increased 2-fold. JDO also had superior intracellular accumulation and excellent pH stability and photostability. By leveraging these advantages, we developed a novel peroxynitrite ($ONOO^-$)-responsive probe, JDO-ONOO, as a proof-of-concept demonstration to validate the design platform. Through strategic disruption of the fluorophore's conjugated structure, JDO-ONOO emitted ultralow background fluorescence, and in the presence of $ONOO^-$, the fluorescence switched to a "turn-on" mode, resulting in a 130-fold increase in intensity. The probe had high sensitivity (LOD = 3.7 nM), rapid response, and excellent selectivity under physiological conditions. It was successfully employed in the fluorescence imaging of $ONOO^-$ in living cells and in multiple mouse models of inflammation. Overall, this study presents a universal strategy for developing next-generation low-background fluorescent probes, demonstrated through $ONOO^-$ detection.

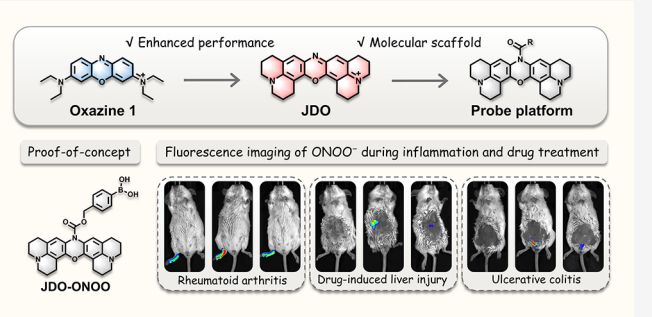

INTRODUCTION

Fluorescent probes are indispensable tools in bioanalysis and biomedical imaging due to their high sensitivity, real-time feedback capability, and noninvasive nature.[1−5] They are often used in the visualization of complex biological processes at the molecular level and have been widely applied in the detection of reactive species, enzymes, ions, and other disease-associated biomarkers.[6−12] However, one of the challenges in the design of fluorescent probes is the presence of background fluorescence under physiological conditions.[13,14] This intrinsic fluorescence, often originating from the probe's native electronic structure or environmental autofluorescence, can significantly reduce the signal-to-noise ratio (SNR), thereby limiting the sensitivity, specificity, and reliability of the probe.[15,16]

To address this issue, recent strategies have focused on designing probes with activatable or "turn-on" fluorescence characteristics, where the fluorescence signal remains quenched until encountering the target analyte.[17−21] Among these strategies, low-background design platforms utilizing the structural disruption of fluorophores to eliminate basal emission have gained considerable attention. In this context, oxazine 1 has emerged as a promising fluorophore scaffold for constructing low-background probes.[22−25] Compared with widely reported fluorophores, Oxazine 1 possesses several favorable characteristics, including near-infrared (NIR) fluorescence emission, high pH stability and modifiability at the central nitrogen atom (Table S1). Moreover, its molecular structure allows for rational disruption and reconstitution of conjugates, making it suitable for constructing activatable probes with low background fluorescence.

Received: July 15, 2025
Revised: September 1, 2025
Accepted: September 16, 2025
Published: September 20, 2025

https://doi.org/10.1021/acs.analchem.5c04331
Anal. Chem. 2025, 97, 21071−21078

Despite these advantages, oxazine 1 has inherent limitations. First, the electron-donating diethylamino group in its structure is relatively weak, thereby limiting a further red shift in the emission spectrum, which is a key requirement for deep-tissue imaging applications.[26] Second, the flexible alkyl chain of the diethylamino group increases intramolecular rotational freedom, facilitating nonradiative decay pathways, which reduce the fluorescence quantum yield.[27] Third, due to the relatively low hydrophobicity of the diethylamino unit, the cellular uptake is limited, resulting in low accumulation in cells and decreased imaging brightness.[28]

To overcome these deficiencies, we proposed a novel structural modification strategy for oxazine 1, in which the original diethylamino group was replaced with a julolidine unit. Julolidine has a rigid, electron-rich cyclic structure that can enhance electron-donating ability, suppress nonradiative decay through conformational restriction, and improve lipophilicity for better cell membrane permeability.[29,30] Based on this strategy, we designed and synthesized two new oxazine-derived fluorophores: JSO (bearing a single julolidine substituent) and JDO (bearing two julolidine substituents). To validate their performance, we systematically examined photophysical properties, including absorption/emission spectra, quantum yield, pH and photostability, and lipophilicity (logP). We also evaluated their biocompatibility, cellular uptake behavior, and imaging performance. Among the two, JDO showed the largest red shift in emission and the highest fluorescence quantum yield and cellular uptake.

To demonstrate the usability of the JDO scaffold in constructing low-background activatable probes, peroxynitrite ($ONOO^-$) was employed as a model analyte. $ONOO^-$, a reactive nitrogen species generated during inflammatory pathologies, was used as a representative model for assessing probe performance due to its high reactivity and short half-life.[31−35] Based on this rationale, we developed JDO-ONOO by covalently linking a phenylboronic acid group to the central nitrogen of JDO to quench the fluorescence of JDO, which occurs through conjugation disruption. Upon $ONOO^-$-mediated cleavage, the conjugated structure of JDO is restored, resulting in a pronounced fluorescence turn-on response. This strategy exemplifies the modularity and efficiency of the JDO-based design because the signal transduction mechanism is embedded within the fluorophore scaffold itself. Importantly, this approach is not limited to $ONOO^-$ detection but can be broadly applied to other analytes. The strategy can be applied in the development of next-generation fluorescent probes with minimal background interference and high signal fidelity under physiological conditions.

EXPERIMENTAL SECTION

Synthesis. The synthesis procedures, nuclear magnetic resonance (NMR) spectra, and high-resolution mass spectrometry (HRMS) data for compounds JSO, JDO, and JDO-ONOO are provided in the Supporting Information.

Photophysical Characterization. Stock solutions of oxazine 1, JSO, JDO, and JDO-ONOO were prepared in DMSO each at a concentration of 1 mM and stored at − 20 °C. Prior to measurements, each stock solution was diluted in phosphate-buffered saline (PBS, 10 mM, pH 7.4) to a final concentration of 10 μM with a total volume of 1 mL. UV−vis absorption spectra were recorded using a UV−vis spectrophotometer, and fluorescence spectra were measured using a fluorescence spectrometer.

Cellular Uptake Analysis. HepG2 cells were incubated with 5 μM of oxazine 1, JSO, or JDO for 20 min at 37 °C. After incubation, the cells were washed three times with PBS (10 mM, pH 7.4) to remove unbound dye. Fluorescence imaging was carried out using a laser scanning confocal microscope under identical conditions.

Flow Cytometry. To quantitatively assess the cellular uptake, HepG2 cells were cultured in 6-well plates for 48 h. The cells were then incubated with 1 μM oxazine 1, JSO, or JDO for 20 min. After incubation, the cells were trypsinized, washed with PBS, and subjected to flow cytometry. Fluorescence intensity data were collected from 10,000 gated events per sample.

RESULTS AND DISCUSSION

Design of Fluorophores. Oxazine 1 is a classical near-infrared fluorophore with a planar conjugated system and excellent pH and photostability. Its central nitrogen atom can be easily modified, making it an attractive scaffold for constructing activatable fluorescent probes. However, several intrinsic limitations restrict its performance in biological applications. First, oxazine 1 contains a diethylamino moiety, an electron-donating group that confers only moderate electron-donating ability. This limits the extent of π-electron delocalization and restricts the red-shifting of its emission spectrum. Second, the flexible alkyl chains of the diethylamino group can undergo intramolecular rotation and vibration, which facilitates nonradiative decay, causing a reduction in fluorescence quantum yield. Third, the short hydrophobic chains contribute marginally to lipophilicity, resulting in suboptimal membrane permeability and inefficient cellular uptake.

To overcome these limitations, we introduced julolidine, a rigid, cyclic amine known for its strong electron-donating ability and low conformational flexibility, into the oxazine 1 core. The design strategy was based on the following three considerations. (1) Electron effect: Julolidine has a stronger electron-donating capability compared to diethylamine due to the fused ring structure that stabilizes the lone pair on the nitrogen atom. The incorporation of julolidine increases the electron density at the donor site and enhances intramolecular charge transfer (ICT) upon excitation. This electronic distribution modulation results in a significant red shift of both absorption and emission wavelengths, making the dyes more suitable for deep-tissue imaging. (2) Structural rigidity: Unlike the flexible diethylamino group, julolidine contains a rigid polycyclic structure with low intramolecular rotation and vibration in the excited state. This conformational constraint effectively reduces the probability of nonradiative decay and facilitates radiative transition, thereby increasing fluorescence quantum yield. (3) Hydrophobicity and cell membrane permeability: The julolidine unit has a larger molecular volume and greater hydrophobic surface area compared to diethylamine. These properties help increase the lipophilicity, thus enhancing the dye's ability to penetrate cell membranes, resulting in improved intracellular accumulation. This increased membrane permeability can enhance imaging brightness and delivery efficiency.

Based on this strategy, two novel oxazine derivatives were synthesized, and the effects of julolidine substitution on their photophysical properties were systematically evaluated. JSO contained a single julolidine unit at a single site, whereas JDO contained julolidine groups at both sites in a symmetrical

https://doi.org/10.1021/acs.analchem.5c04331
Anal. Chem. 2025, 97, 21071−21078

fashion. This structural progression from mono- to disubstitution allows for dose-dependent modulation of electron-donating strength and conjugation degree. The chemical structures of oxazine 1, JSO, and JDO are shown in Figure 1A.

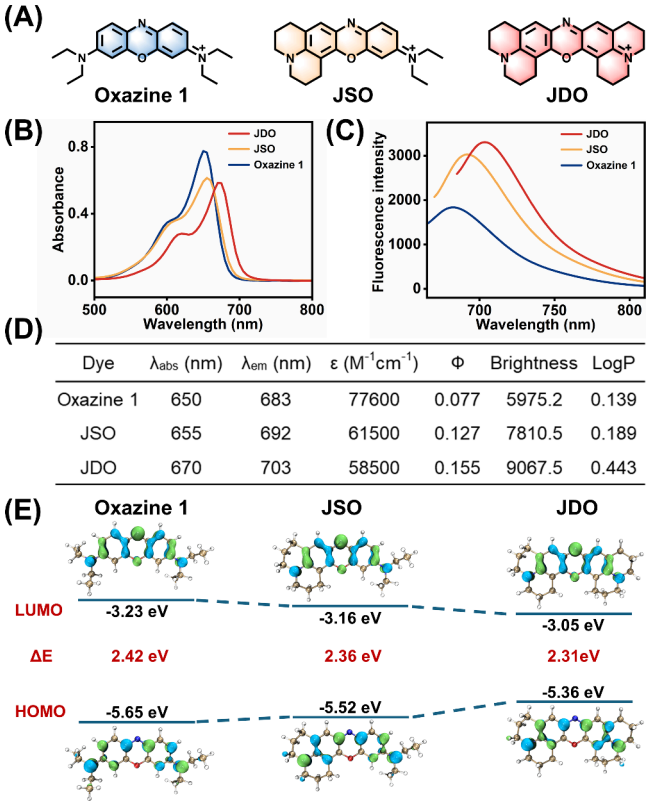

Dye	λ_{abs} (nm)	λ_{em} (nm)	ε ($M^{-1}cm^{-1}$)	Φ	Brightness	LogP
Oxazine 1	650	683	77600	0.077	5975.2	0.139
JSO	655	692	61500	0.127	7810.5	0.189
JDO	670	703	58500	0.155	9067.5	0.443

Figure 1. (A) Chemical structures of oxazine 1, JSO, and JDO. (B) Absorption spectra of oxazine 1, JSO, and JDO (10 μM) in aqueous solution. (C) Fluorescence spectra of oxazine 1, JSO, and JDO (10 μM) in aqueous solution. The excitation wavelength was selected at the maximum absorption wavelength of the respective dye. (D) Various photophysical properties of oxazine 1, JSO, and JDO in aqueous solution. (E) Theoretical simulation of oxazine 1, JSO, and JDO.

Characterization of Photophysical Properties. We evaluated the performance of oxazine 1, JSO, and JDO by systematically investigating and comparing their photophysical properties.

UV–vis Absorption and Fluorescence Emission. The absorption and fluorescence spectra of JSO and JDO were examined in various solvents (Figures S1–S4). Compared with oxazine 1, which has a maximum absorption at 650 nm and a maximum emission at 683 nm, the spectra of both JSO and JDO were drastically red-shifted in aqueous solution. Specifically, the largest shift was observed in JDO, with a maximum absorption at 670 nm and a maximum emission at 703 nm (Figures 1B,1C). These results indicate that julolidine substitution effectively expands the π-conjugation and enhances ICT, thus improving spectra, making them suitable for *in vivo* imaging applications.

Fluorescence Quantum Yield and Brightness. The fluorescence quantum yields (Φ) of oxazine 1, JSO, and JDO were determined using an absolute measurement method with an integrating sphere. The Φ values of oxazine 1, JSO, and JDO in aqueous solution were 0.077, 0.127, and 0.155, respectively. The enhancement in quantum yield is likely attributed to the rigidity introduced by the julolidine moiety, which effectively suppresses nonradiative decay pathways by restricting intramolecular rotations and vibrations in the excited state. The increase in radiative efficiency results in greater fluorescence brightness (Figure 1D).

Theoretical Calculations. To gain insights into the electronic origins of the observed spectral shifts and quantum yield enhancement, density functional theory (DFT) calculations were applied. The results showed that julolidine substitution elevated the HOMO energy level while simultaneously lowering the LUMO, thereby narrowing the HOMO–LUMO gap (Figure 1E). The reduction in the band gap energy causes a red shift in the excitation and emission wavelengths.

Lipophilicity Assessment (logP). To assess hydrophobicity, we measured the octanol–water partition coefficient (logP) of each dye. Compared with that of oxazine 1, the logP value of JSO and JDO was 1.36-fold and 3.19-fold higher, respectively (Figure 1D). This result is consistent with the introduction of larger, more hydrophobic julolidine groups, which help increase the membrane permeability and enhance the intracellular delivery efficiency.

PH Stability and Photostability. The ability of the dye to maintain its fluorescence performance under varying physiological conditions is essential for biological applications. Both JSO and JDO had excellent pH tolerance and photostability. At pH ranging from 3.0 to 9.0 and under continuous illumination, the emission intensity was not significantly changed (Figures S5–S6), and the fluorescence signals remained stable (Figures S7–S8). These results indicate that julolidine substitution has no impact on the photostability of the dye, further supporting their suitability in live-cell and *in vivo* imaging.

Biocompatibility and Cytotoxicity. JSO and JDO showed excellent stability in DMEM medium (containing 10% FBS) (Figures S9–S10). The cytocompatibility of JSO and JDO was evaluated using the CCK-8 assay. Both dyes showed negligible cytotoxicity at concentrations up to 50 μM, consistent with their structural neutrality and lack of reactive moieties (Figures S11–S12). With such excellent biocompatibility, they are suitable for further biological and biomedical applications.

Cellular Uptake and Imaging Performance. To examine intracellular distribution, HepG2 cells were incubated with 5 μM of each dye for 20 min and then subjected to confocal fluorescence imaging. Oxazine 1 exhibited weak intracellular signals, indicating poor uptake. In contrast, JDO showed the brightest fluorescence, with uniform intracellular distribution. JSO produced moderate signal levels (Figures 2A,2B). The fluorescence intensity was further quantified by flow cytometry. The fluorescence intensity of the JDO group was significantly higher than that of the JSO and oxazine 1 groups. (Figure 2C).

Taken together, these results demonstrate that julolidine substitution can substantially enhance spectral properties, brightness, cellular uptake, and imaging contrast of the fluorophore. Among the two derivative dyes, JDO showed the most promising profile and was therefore selected as the scaffold for subsequent probe development.

Proof-of-Concept of Probe Platform. Building on the superior photophysical and biological properties of JDO, we sought to demonstrate its potential as a universal scaffold for constructing next-generation low-background fluorescent probes. The key design principle was to functionalize the

https://doi.org/10.1021/acs.analchem.5c04331
Anal. Chem. 2025, 97, 21071–21078

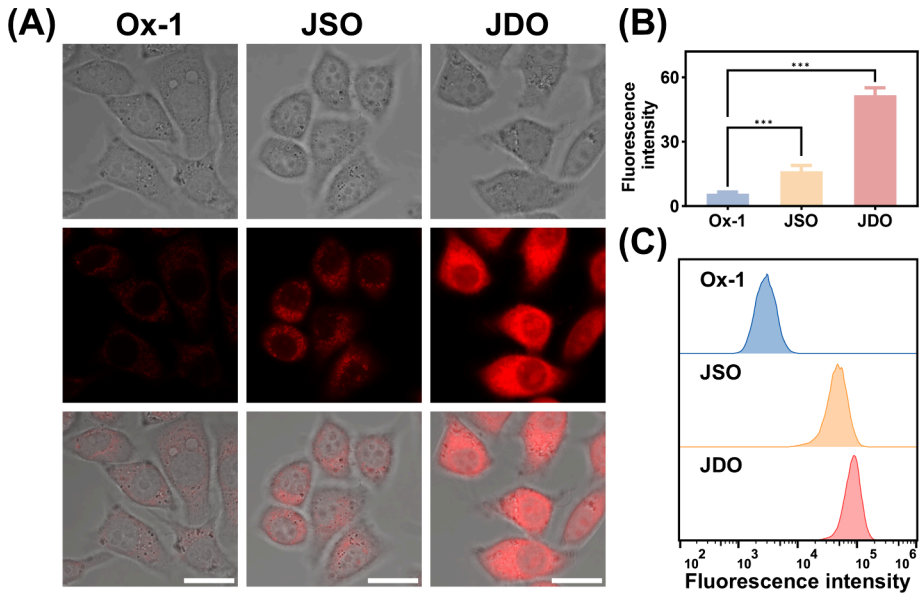

Figure 2. (A) Fluorescence images of HepG2 cells incubated with oxazine 1, JSO, or JDO (5 μM). (B) Comparison of fluorescence intensities of images in (A). (C) Flow cytometry analysis of HepG2 cells after incubation with oxazine 1, JSO, or JDO (1 μM). All fluorescence images were acquired at λ_{ex} = 640 nm and λ_{em} = 663−738 nm. Scale bar: 20 μm. Data were shown as mean ± SD (n = 3, one-way ANOVA, ***p < 0.001).

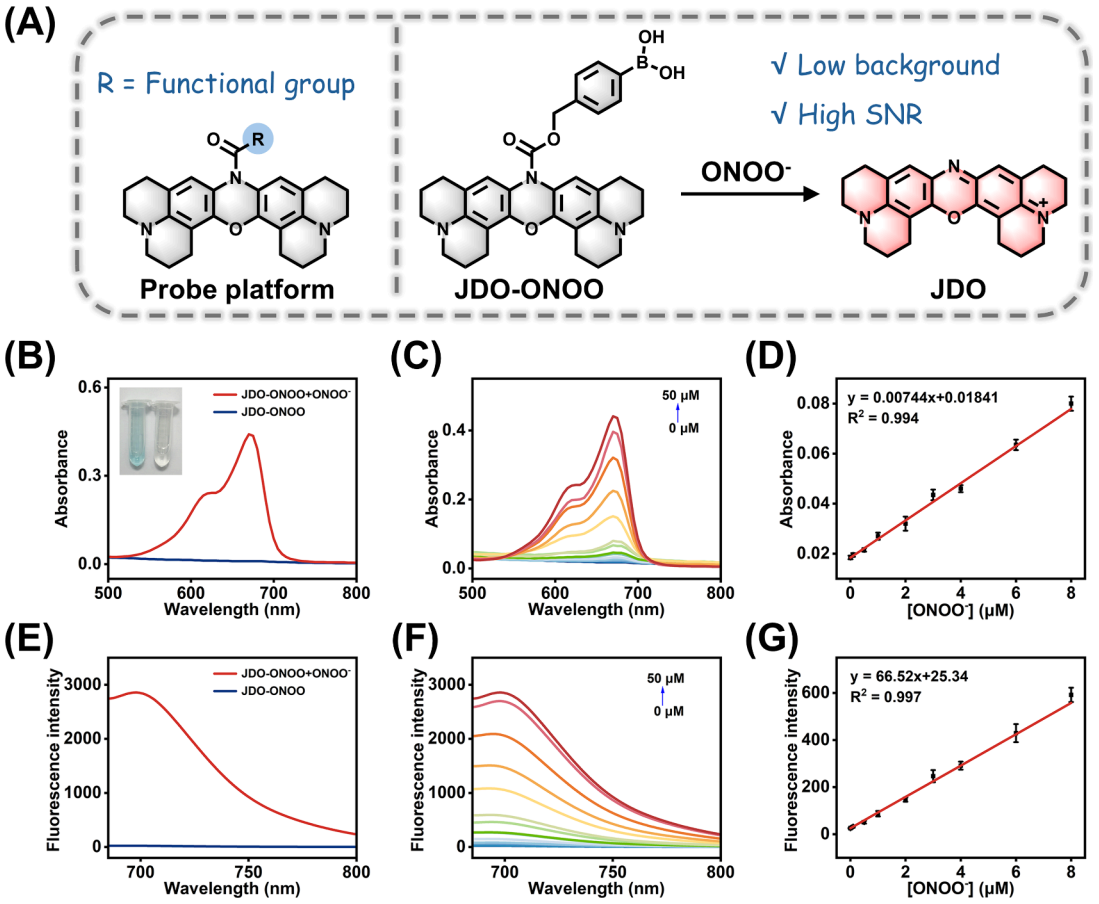

Figure 3. (A) Schematic illustration of JDO (a platform for next-generation low-background fluorescent probes) and the design of JDO-ONOO probe. (B) Absorption spectra of JDO-ONOO (10 μM) before and after the addition of $ONOO^-$ (50 μM). (C) Absorption spectra of JDO-ONOO (10 μM) in the presence of $ONOO^-$ at varying concentrations. (D) Linear correlation between absorbance and $ONOO^-$ concentration (0.01 − 8 μM). (E) Fluorescence spectra of JDO-ONOO (10 μM) before and after the addition of $ONOO^-$ (50 μM). (F) Fluorescence spectra of JDO-ONOO (10 μM) in the presence of $ONOO^-$ at varying concentrations. (G) Linear correlation between fluorescence intensity (λ_{ex} = 670 nm) and $ONOO^-$ concentration (0.01 − 8 μM).

https://doi.org/10.1021/acs.analchem.5c04331
Anal. Chem. 2025, 97, 21071−21078

fluorophore's central nitrogen atom to disrupt the conjugated π-system to achieve a fully quenched, zero-background fluorophore prior to activation. Upon interacting with a specific analyte, the quenching moiety is cleaved, the conjugation is restored, and the fluorescence is turned on ("turn-on" response). This strategy not only eliminates background signals but also significantly enhances the signal-to-noise ratio and thus is a robust framework for sensitive and specific detection of analytes. To validate this concept, we selected $ONOO^-$ as a model target and designed the activatable probe JDO-ONOO. $ONOO^-$ is a highly reactive nitrogen species involved in a variety of inflammatory pathologies, making it a biologically relevant and challenging analyte for detection. For the recognition element, we introduced a phenylboronic acid, which is a well-known $ONOO^-$-responsive group, at the central nitrogen site of JDO. This substitution effectively disrupts the electron delocalization pathway and suppresses fluorescence during the unreacted state (Figure 3A).

Spectroscopic Response to $ONOO^-$. Upon the addition of $ONOO^-$ (50 μM) to a PBS solution (10 μM JDO-ONOO, pH 7.4), the initially colorless and nonfluorescent probe solution rapidly turned blue, accompanied by the appearance of distinct UV−vis absorption and fluorescence emission peaks at 670 and 703 nm, respectively (Figures 3B,3E). These dramatic spectral changes suggest that $ONOO^-$ effectively cleaves the phenylboronic acid, leading to the release of the parent fluorophore JDO and the restoration of its extended conjugated system. Mass spectrometry analysis of the mixture postreaction confirmed that JDO was formed, as evidenced by the appearance of its characteristic molecular ion peaks (Figure S13). This observation provides direct evidence of the fluorophore recovery mechanism. This structural reconstitution ensures that the emission of fluorescence only occurs upon specific activation, resulting in minimal background fluorescence.

Quantitative Detection Performance. We further evaluate the quantitative detection performance of JDO-ONOO by titrating it with $ONOO^-$ at various concentrations. Both the absorption and fluorescence intensities increased proportionally with increasing $ONOO^-$ concentration, and the correlations had excellent linearity (Figures 3C,3D,3F,3G). The calculated detection limit was 5.1 nM for absorption and 3.7 nM for fluorescence, indicative of the high sensitivity and suitability for quantitative detection of the probe.

Response Kinetics and Stability. Time-dependent fluorescence measurements showed that the intensity reached a plateau within minutes after the addition of $ONOO^-$, which is demonstrative of rapid reaction kinetics (Figure S14). Such a rapid response is essential for real-time detection in dynamic biological systems. In addition, the probe was able to retain its photostability upon continuous excitation and to maintain spectral stability across a broad pH range (pH 3.0−9.0), which confirms its robustness in diverse physiological environments (Figures S15−S16).

Selectivity and Specificity. Given that various active substances in biological systems may interfere with the probe, we conducted experiments to determine the selectivity of JDO-ONOO (Figure S17). The results indicated that the fluorescence of JDO-ONOO was significantly enhanced only after incubating with $ONOO^-$. This demonstrates that JDO-ONOO possesses excellent selectivity toward $ONOO^-$.

In summary, JDO-ONOO possesses all the hallmarks of a high-performance activatable fluorescent probe: low background, high SNR, fast and sensitive response, and excellent selectivity. $ONOO^-$ was only chosen for initial demonstration; the modular design of the JDO scaffold allows for substitution with other recognition groups, which can pave the way for the development of a broad class of low-background probes targeting diverse biological analytes.

Probe Validation in Cell and Animal Models. Encouraged by its favorable spectroscopic properties and high selectivity, we next evaluated the applicability of JDO-ONOO in imaging $ONOO^-$ in living systems. A series of cellular and animal experiments were conducted to validate biocompatibility, target responsiveness, and imaging performance of the probe under physiological and pathological conditions.

Fluorescence Imaging of $ONOO^-$ in Living Cells. Prior to cellular imaging, the cytotoxicity of JDO-ONOO was assessed using the CCK-8 assay. The probe exhibited minimal cytotoxicity across the tested concentrations (Figure S18), indicative of high biocompatibility and suitability for biological applications. To confirm its $ONOO^-$-responsiveness in cells, we performed a classical donor-scavenger assay. Exogenous $ONOO^-$ was generated using 3-morpholinosydnonimine hydrochloride (SIN-1), and uric acid (UA) was used as an $ONOO^-$ scavenger. As shown in Figures 4A and 4C, SIN-1

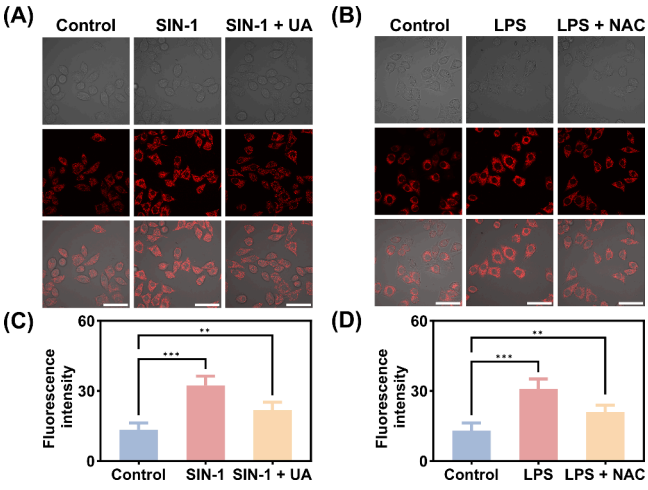

Figure 4. (A) Fluorescence images of cells treated with SIN-1 (300 μM) and SIN-1 (300 μM) + UA (100 μM). (B) Fluorescence images of cells treated with LPS (5 μg/mL) and LPS (5 μg/mL) + NAC (1 mM). (C) Comparison of fluorescence intensities for images in (A). (D) Comparison of fluorescence intensities for images in (B). All fluorescence images were acquired at λ_{ex} = 640 nm and λ_{em} = 663−738 nm. Scale bar: 50 μm. Data were shown as mean ± SD (n = 3, one-way ANOVA, $^{**}p < 0.01$, $^{***}p < 0.001$).

treatment resulted in a marked increase in intracellular fluorescence, while UA pretreatment significantly attenuated the signal. These results confirm that the fluorescence activation of JDO-ONOO is specifically mediated by $ONOO^-$ in the cellular environment. We further applied JDO-ONOO to detect endogenous $ONOO^-$ production in an inflammation cell model induced by lipopolysaccharide (LPS). Compared to that of untreated cells (control), the fluorescence signal of LPS-stimulated cells was significantly enhanced, an indication of elevated $ONOO^-$ levels under inflammatory

https://doi.org/10.1021/acs.analchem.5c04331
Anal. Chem. 2025, 97, 21071−21078

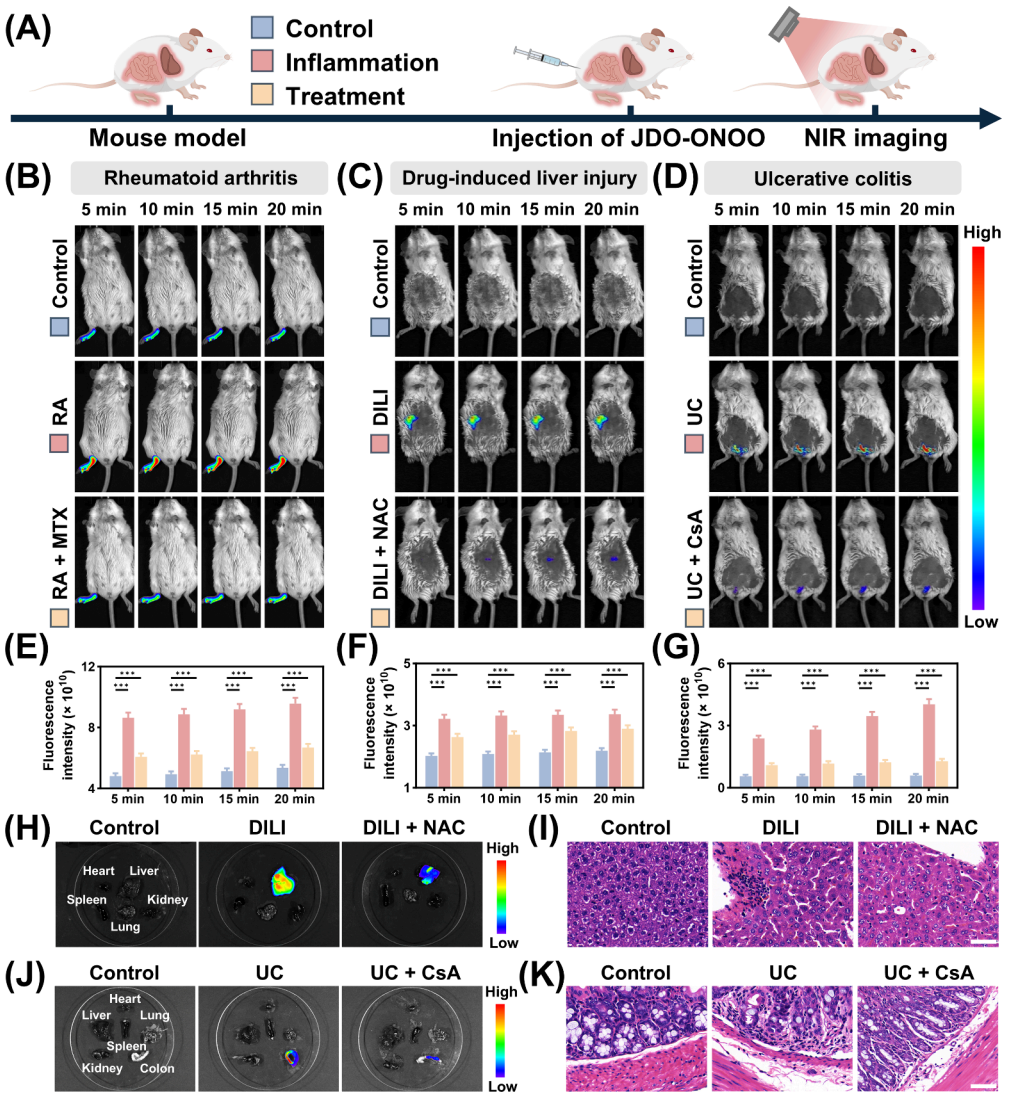

Figure 5. (A) Schematic diagram of different mouse models for in vivo fluorescence imaging. (B) Fluorescence images of control, RA, and RA + MTX-treated mice at different time points following JDO-ONOO injection. (C) Fluorescence images of control, DILI, and DILI + NAC-treated mice at different time points following JDO-ONOO injection. (D) Fluorescence images of control, UC, and UC + CsA-treated mice at different time points following JDO-ONOO injection. (E) Mean fluorescence intensity from the images in (B). (F) Mean fluorescence intensity from the images in (C). (G) Mean fluorescence intensity from the images in (D). (H) Ex vivo fluorescence images of dissected organs of mice in (C). (I) H&E staining images of liver tissue of mice in (C). (J) Ex vivo fluorescence images of dissected organs of mice in (D). (K) H&E staining images of colon tissue of mice in (D). Scale bar: 50 μm. Data were shown as mean ± SD (n = 3, two-way ANOVA, ***p < 0.001).

conditions. Treatment with the antioxidant N-acetylcysteine (NAC) led to a substantial reduction in fluorescence intensity (Figures 4B,4D), which further validates the probe's responsiveness to fluctuations in $ONOO^-$ content. These findings demonstrate that JDO-ONOO can reliably and sensitively detect the dynamic changes in $ONOO^-$ content in live cells; thus, it is a promising tool for inflammation monitoring and drug evaluation.

Fluorescence Imaging of $ONOO^-$ in Mouse Models. To extend its applications to *in vivo* settings, we applied JDO-ONOO to detect $ONOO^-$ in three disease models involving $ONOO^-$ dysregulation, including rheumatoid arthritis (RA), drug-induced liver injury (DILI), and ulcerative colitis (UC) (Figure 5A).[36−41]

RA Model. In a λ-carrageenan-induced mouse model of RA, intra-articular injection of JDO-ONOO revealed significantly enhanced fluorescence signals in the inflamed joints compared to healthy controls. The increase in fluorescence signals reflects the local accumulation of $ONOO^-$ during inflammation. Treatment with methotrexate (MTX), a commonly used clinical drug for the treatment of RA, resulted in a notable decrease in fluorescence intensity (Figures 5B,5E). These findings demonstrate that JDO-ONOO can effectively monitor $ONOO^-$ in inflamed tissues and assess the effectiveness of therapeutic interventions.

DILI Model. In a mouse model of acetaminophen (APAP)-induced liver injury, JDO-ONOO was successfully employed in real-time imaging of hepatic $ONOO^-$ elevation. Fluorescence intensity in the liver was significantly higher in DILI mice compared to controls, consistent with the known elevation of $ONOO^-$ due to hepatocellular damage. Following NAC treatment, $ONOO^-$ levels were markedly reduced, as indicated by decreased hepatic fluorescence (Figures 5C,5F). *Ex vivo* imaging further confirmed liver-localized fluorescence

https://doi.org/10.1021/acs.analchem.5c04331
Anal. Chem. 2025, 97, 21071−21078

(Figure 5H), and histological analysis via H&E staining showed that changes in $ONOO^-$ levels were correlated with the extent of tissue damage and recovery (Figure 5I).

UC Model. In a dextran sulfate sodium (DSS)-induced mouse model of ulcerative colitis, JDO-ONOO revealed a significant upregulation of $ONOO^-$ content in inflamed colon tissues. Administration with cyclosporin A (CsA) led to a substantial reduction in fluorescence intensity, consistent with the suppressed $ONOO^-$ production after treatment (Figures 5D,5G). *Ex vivo* imaging further showed that the fluorescence was localized exclusively in the colonic region (Figure 5J), and H&E staining confirmed that the alleviation of histopathological damage was mediated by CsA (Figure 5K). These results demonstrate that JDO-ONOO is a robust tool for assessing the inflammatory status and treatment efficacy in intestinal diseases.

Collectively, these *in vivo* results confirm that JDO-ONOO possesses excellent biocompatibility and high sensitivity and is responsive to $ONOO^-$. The probe can be used for real-time, low-background fluorescence imaging of various inflammation-related disease models and for assessing the efficacy of therapeutic interventions. These findings not only validate the suitability for practical applications of the JDO-based platform but also highlight its potential in a broad range of biological sensing and disease monitoring.

CONCLUSIONS

In this study, we report a fluorophore engineering strategy that addresses key limitations of oxazine 1, including short emission wavelength, low fluorescence quantum yield, and poor cellular uptake, by introducing julolidine as an electron-donating unit. Through structural modification, we successfully developed two new oxazine-based dyes: JSO (monojulolidine) and JDO (dijulolidine). These fluorophores inherited the high pH stability and photostability of oxazine 1, while gaining three new, enhanced photophysical properties: (i) significant red-shifted fluorescence emission (up to 703 nm), (ii) markedly increased fluorescence quantum yield, and (iii) greatly improved cellular uptake (due to enhanced lipophilicity). Among the two fluorophores, JDO had the most favorable optical and biological performance and was therefore selected as the prototype scaffold for constructing a next-generation low-background probe platform. As a proof-of-concept, we designed and synthesized JDO-ONOO, a peroxynitrite-responsive activatable fluorescent probe. By selectively modifying its central nitrogen atom to disrupt the conjugated system, JDO-ONOO exhibited "zero-background" fluorescence prior to activation but generated a strong turn-on fluorescence signal upon activation by $ONOO^-$. The probe had excellent sensitivity (with LOD as low as 3.7 nM), rapid kinetics, and high selectivity in various complex biological matrices. These properties validate the effectiveness of the proposed conjugation disruption and recovery-based design strategy. It is important to note that $ONOO^-$ was selected as a representative target to verify the performance of the JDO-based platform. The innovation in this study lies not only in $ONOO^-$ detection but also in establishing a universal strategy for developing high-performance, activatable fluorescent probes with minimal background signals. The developed JDO fluorophore is a modular, robust, and versatile scaffold that can readily be attached to other recognition moieties specific to other biological targets, which can include reactive species, enzymes, ions, and other disease-associated biomarkers. We hope that this work will inspire the development of other low-fluorescence-background imaging tools for a broad range of applications, such as early disease diagnosis, real-time monitoring of pathophysiological processes, and evaluation of therapeutic efficacy.

ASSOCIATED CONTENT

Supporting Information

The Supporting Information is available free of charge at https://pubs.acs.org/doi/10.1021/acs.analchem.5c04331.

Additional experimental details, including materials and instruments, determination of the detection limit, synthesis, cellular experiments, mouse experiments, and supplementary Figures (PDF)

AUTHOR INFORMATION

Corresponding Authors

Pinyi Ma − *College of Chemistry, Jilin Province Research Center for Engineering and Technology of Spectral Analytical Instruments, Jilin University, Changchun 130012, China;* orcid.org/0000-0002-3230-4928; Email: mapinyi@jlu.edu.cn

Bo Zhang − *International Center of Future Science, Jilin University, Changchun 130012, China;* Email: bozhang2019@jlu.edu.cn

Daqian Song − *College of Chemistry, Jilin Province Research Center for Engineering and Technology of Spectral Analytical Instruments, Jilin University, Changchun 130012, China;* orcid.org/0000-0002-4866-1292; Email: songdq@jlu.edu.cn

Authors

Dianfeng Dai − *College of Chemistry, Jilin Province Research Center for Engineering and Technology of Spectral Analytical Instruments, Jilin University, Changchun 130012, China*

Zhimin Zhang − *Department of Pharmacy, Changchun Medical College, Changchun 130031, China*

Mo Ma − *College of Chemistry, Jilin Province Research Center for Engineering and Technology of Spectral Analytical Instruments and School of Pharmacy, Jilin University, Changchun 130012, China*

Chen Zhao − *College of Chemistry, Jilin Province Research Center for Engineering and Technology of Spectral Analytical Instruments, Jilin University, Changchun 130012, China*

Jingkang Li − *College of Chemistry, Jilin Province Research Center for Engineering and Technology of Spectral Analytical Instruments, Jilin University, Changchun 130012, China*

Siqi Zhang − *College of Chemistry, Jilin Province Research Center for Engineering and Technology of Spectral Analytical Instruments, Jilin University, Changchun 130012, China*

Complete contact information is available at: https://pubs.acs.org/10.1021/acs.analchem.5c04331

Notes

The authors declare no competing financial interest.

ACKNOWLEDGMENTS

This work was supported by the National Natural Science Foundation of China (22074052 and 22004046) and the Science and Technology Developing Foundation of Jilin Province of China (20250206038ZP).

REFERENCES

(1) Zhou, Y.; Yang, X.; Lee, H.; Yan, M.; Yoon, J. *Coordin. Chem. Rev.* **2025**, *541*, No. 216785.
(2) Jing, X.; Han, S.; Yang, Y.; Lai, Y.; Lin, W. *Coordin. Chem. Rev.* **2025**, *534*, No. 216607.
(3) Wang, X.; Ding, Q.; Groleau, R. R.; Wu, L.; Mao, Y.; Che, F.; Kotova, O.; Scanlan, E. M.; Lewis, S. E.; Li, P.; Tang, B.; James, T. D.; Gunnlaugsson, T. *Chem. Rev.* **2024**, *124*, 7106−7164.
(4) Fujita, K.; Urano, Y. *Chem. Rev.* **2024**, *124*, 4021−4078.
(5) Meng, W.; Chen, R.; Jang, Q.; Ma, K.; Li, D.; Xiao, H.; Chi, W.; Zeng, C.; Shu, W. *Coordin. Chem. Rev.* **2025**, *529*, No. 216456.
(6) Geng, Y.; Wang, Z.; Zhou, J.; Zhu, M.; Liu, J.; James, T. D. *Chem. Soc. Rev.* **2023**, *52*, 3873−3926.
(7) Kim, J.; Nimse, S. B. *Coordin. Chem. Rev.* **2025**, *537*, No. 216690.
(8) Zhang, S.-S.; Kim, H.; Zhou, Y.; Kang, H.; Yoon, J. *TrAC, Trends Anal. Chem.* **2025**, *185*, No. 118165.
(9) Grover, K.; Koblova, A.; Pezacki, A. T.; Chang, C. J.; New, E. J. *Chem. Rev.* **2024**, *124*, 5846−5929.
(10) Zhang, R.-W.-Y.; Zhang, H.; Li, Q.; Li, F.-P.; Zhang, R.-Y.; Zhao, W.-B.; Liu, H.-J.; Hu, Z.-G.; Wang, K. *Coordin. Chem. Rev.* **2025**, *529*, No. 216471.
(11) Sharma, A.; Verwilst, P.; Li, M.; Ma, D.; Singh, N.; Yoo, J.; Kim, Y.; Yang, Y.; Zhu, J.-H.; Huang, H.; Hu, X.-L.; He, X.-P.; Zeng, L.; James, T. D.; Peng, X.; Sessler, J. L.; Kim, J. S. *Chem. Rev.* **2024**, *124*, 2699−2804.
(12) Wu, X. F.; Wang, R.; Kwon, N.; Ma, H. M.; Yoon, J. *Chem. Soc. Rev.* **2022**, *51*, 450−463.
(13) Wu, F. P.; Zheng, B. B.; Qiu, X. Y.; Hu, T.; Yang, Y. X.; Yang, K. R.; Zhou, B. J.; Ma, Q.; Pang, D. W.; Xiong, H. *Angew. Chem., Int. Ed.* **2025**, No. e202423059.
(14) Dai, D.; Zhang, Z.; Ma, M.; Li, J.; Zhang, S.; Ma, P.; Song, D. *Anal. Chem.* **2025**, *97*, 1402−1409.
(15) Zeng, Q.; Yuwen, Z.; Zhang, L.; Li, Y.; Liu, H.; Zhang, K. *Anal. Chem.* **2024**, *96*, 13260−13269.
(16) Jiang, G. W.; Liu, H.; Deng, G. H.; Liu, H.; Zhou, Z. X.; Ren, T. B.; Wang, L.; Zhang, X. B.; Yuan, L. *Angew. Chem., Int. Ed.* **2024**, *63*, No. e202400637.
(17) Numasawa, K.; Hanaoka, K.; Saito, N.; Yamaguchi, Y.; Ikeno, T.; Echizen, H.; Yasunaga, M.; Komatsu, T.; Ueno, T.; Miura, M.; Nagano, T.; Urano, Y. *Angew. Chem., Int. Ed.* **2020**, *59*, 6015−6020.
(18) Wu, L.; Li, Z.; Wang, K.; Groleau, R. R.; Rong, X.; Liu, X.; Liu, C.; Lewis, S. E.; Zhu, B.; James, T. D. *J. Am. Chem. Soc.* **2025**, *147*, 9001−9018.
(19) Li, H. Y.; Luo, X.; Jian, Y.; Lv, J. J.; Li, X. M.; Gao, J.; Shi, W.; Li, X. H.; Yuan, Z. L.; Ma, H. M. *Chem. Sci.* **2025**, *16*, 4136−4143.
(20) Zhou, Y.; Yang, X.; Jang, W. J.; Yan, M.; Yoon, J. *Coordin. Chem. Rev.* **2025**, *522*, No. 216201.
(21) Ding, C.; Ren, T. *Coordin. Chem. Rev.* **2023**, *482*, No. 215080.
(22) Wen, Y.; Hu, Z.; Tian, W.; Yan, H.; Huo, F.; Yin, C. *Biomaterials.* **2025**, *322*, No. 123382.
(23) Wen, Y.; Jing, N.; Zhang, M.; Huo, F. J.; Li, Z. Y.; Yin, C. X. *Adv. Sci.* **2023**, *10*, No. 2206681.
(24) Shang, J. Z.; Zhang, X. F.; He, Z. X.; Shen, S. L.; Liu, D. K.; Shi, W.; Ma, H. M. *Angew. Chem., Int. Ed.* **2022**, *61*, No. e202205043.
(25) Dai, D.; Zhang, Z.; Ma, M.; Zhao, C.; Li, J.; Zhang, S.; Ma, P.; Wu, Q.; Song, D. *Anal. Chem.* **2025**, *97*, 9414−9421.
(26) Jiang, G. W.; Liu, H.; Liu, H.; Ke, G. L.; Ren, T. B.; Xiong, B.; Zhang, X. B.; Yuan, L. *Angew. Chem., Int. Ed.* **2024**, *63*, No. e202315217.
(27) Wang, C.; Qiao, Q. L.; Chi, W. J.; Chen, J.; Liu, W. J.; Tan, D.; McKechnie, S.; Lyu, D.; Jiang, X. F.; Zhou, W.; Xu, N.; Zhang, Q. S.; Xu, Z. C.; Liu, X. G. *Angew. Chem., Int. Ed.* **2020**, *59*, 10160−10172.
(28) Jiang, G. W.; Lou, X. F.; Zuo, S.; Liu, X. X.; Ren, T. B.; Wang, L.; Zhang, X. B.; Yuan, L. *Angew. Chem., Int. Ed.* **2023**, *62*, No. e202218613.
(29) Liu, C.; Cai, Y.; Zhang, Z.; Lu, Y.; Zhu, Q.; He, H.; Chen, Z.; Zhao, W.; Wu, W. *Acta. Pharm. Sin. B* **2024**, *14*, 3155−3168.
(30) Qi, Q.; Liu, Y.; Puranik, V.; Patra, S.; Svindrych, Z.; Gong, X.; She, Z.; Zhang, Y.; Aprahamian, I. *J. Am. Chem. Soc.* **2025**, *147*, 16404−16411.
(31) Liu, G.; Xie, X.; Li, Y.; Zhang, J.; Jiao, X.; Dou, X.; Wang, X.; Tang, B. *TrAC, Trends Anal. Chem.* **2023**, *169*, No. 117371.
(32) Zhou, Y.; Yang, X.; zhang, J.; Xu, S.; Li, J.; Wang, W.; Yan, M. *Coordin. Chem. Rev.* **2023**, *493*, No. 215258.
(33) Cui, W.-L.; Wang, M.-H.; Yang, Y.-H.; Wang, J.-Y.; Zhu, X.; Zhang, H.; Ji, X. *Coordin. Chem. Rev.* **2023**, *474*, No. 214848.
(34) Mao, Z.; Xiong, J.; Wang, P.; An, J.; Zhang, F.; Liu, Z.; Seung Kim, J. *Coordin. Chem. Rev.* **2022**, *454*, No. 214356.
(35) Wang, S.; Chen, L.; Jangili, P.; Sharma, A.; Li, W.; Hou, J.-T.; Qin, C.; Yoon, J.; Kim, J. S. *Coordin. Chem. Rev.* **2018**, *374*, 36−54.
(36) Luo, P.; Gao, F.-Q.; Sun, W.; Li, J.-Y.; Wang, C.; Zhang, Q.-Y.; Li, Z.-Z.; Xu, P. *Mil. Med. Res.* **2023**, *10*, 31.
(37) Pang, Q.; Huo, F.; Yue, Y.; Yin, C. *Chin. Chem. Lett.* **2025**, *36*, No. 110713.
(38) Jaeschke, H.; Ramachandran, A. *Annu. Rev. Pathol.:Mech. Dis.* **2024**, *19*, 453−478.
(39) Wu, L. L.; Liu, J. H.; Tian, X.; Groleau, R. R.; Bull, S. D.; Li, P.; Tang, B.; James, T. D. *Chem. Sci.* **2021**, *12*, 3921−3928.
(40) Kimura, H.; Hokari, R.; Miura, S.; Shigematsu, T.; Hirokawa, M.; Akiba, Y.; Kurose, I.; Higuchi, H.; Fujimori, H.; Tsuzuki, Y.; Serizawa, H.; Ishii, H. *Gut* **1998**, *42*, 180−187.
(41) Zhang, H.; Chen, S.-S.; Wang, Z.-Q.; Mi, J.-F.; Mao, G.-J.; Ouyang, J.; Hu, L.; Li, C.-Y. *Anal. Chem.* **2024**, *96*, 18852−18858.

https://doi.org/10.1021/acs.analchem.5c04331
Anal. Chem. 2025, 97, 21071−21078